Tribology International 135 (2019) 344–354

Contents lists available at ScienceDirect

Tribology International

journal homepage: www.elsevier.com/locate/triboint

# A homogenized micro-elastohydrodynamic lubrication model: Accounting for non-negligible microscopic quantities

Hugo M. Checo[a,b], David Dureisseix[a], Nicolas Fillot[a,*], Jonathan Raisin[b]

[a] Univ Lyon, INSA-Lyon, CNRS UMR5259, LaMCoS, F-69621, France
[b] Research Center of Solaize (CRES), Total Marketing Services, Solaize, France

ARTICLE INFO

*Keywords:*
Homogenization
Elastohydrodynamic lubrication
Microelastohydrodynamic
Roughness*MSC:*
74F10
76D08
35B27
41A60

ABSTRACT

In rough elastohydrodynamic lubricated contacts the geometry often exhibits two clearly separated scales: a macroscopic scale –the one of the bearing– and a microscopic scale, that of the surface roughness. In numerical simulation of lubricated contacts, this difference in scales leads to large systems of equations to solve. Assuming periodicity or pseudo-periodicity of the small scale, several methods to decouple the macro scale from the micro scale have been proposed, the formal approach being the homogenization theory. However, the approximation errors due to the classical asymptotic assumptions can be considerable. In this work we introduce a homogenized model which takes into account the non-negligible pressures and deformations of the micro scale, thus extending the applicability of the classical asymptotic homogenized approaches.

Nomenclature

| | | |
|---|---|---|
| $h$ | $H$ | film thickness |
| $\delta$ | $\Delta$ | elastic body surface normal displacement |
| $l$ | $\varepsilon$, $\varepsilon_0$ | roughness wavelength |
| | $A$ | roughness amplitude |
| $\xi$ | $\xi$ | roughness phase |
| $u_m$ | $\bar{u}$ | entrainment velocity |
| $W$ | | normal load per unit width |
| $\underline{\delta}$ | $\underline{\Delta}$ | displacement field in the equivalent solid |
| $p$ | $P$ | pressure |
| $\rho$ | $\bar{\rho}$ | fluid density |
| $\eta$ | $\bar{\eta}$ | fluid viscosity |
| $R$ | | equivalent curvature radius |
| $a$ | | contact half-width of Hertzian theory |
| $p_h$ | | maximum pressure of Hertzian theory |
| $\frac{\rho h^3}{12\eta}$ | $\varepsilon$ | constitutive parameter |
| $x_1$ | $X_1$ | slow tangential spatial variable |
| | $Y_1$ | fast tangential spatial variable |
| | $M$, $L$ | Moes-Venner parameters |

The symbol in the second column is the non-dimensional version of the one in the first column.

## 1. Introduction

Surface roughness has an impact on lubricated contacts, especially for those operating in severe conditions. Understanding the influence of the microgeometry of the surfaces in contact in the elastohydrodynamic (EHL) regime is essential for the design of improved bearings and mechanical transmissions. From the numerical point of view this constitutes a challenge, given the physics involved and the difference in scales imposed by the geometry of the bearing and the one of the surface roughness. This problem has been handled in two ways: a direct resolution of the problem up to the microscopic scale, which is called in the literature the *deterministic* approach, and also by means of averaging methods. A recent paper by Pei et al. [1] develops a deterministic multiscale computational method (finite cell method, FCM) to solve rough lubricated contacts; it is however limited to conformal hydrodynamics contacts.

As pointed out by Gropper et al. [2], direct simulation becomes too costly for state of the art simulations of EHL contacts, and thus it is restricted to very small domains, such as Hertzian contacts. State of the art modeling involves non-Newtonian fluids, thermal (TEHL) and piezoviscous effects as well as solid deformations for problems that are innately transient. This leads to hundreds of thousands of degrees of freedom, as well as very fine discretizations in time in order to capture the characteristic times of the problem [3]. Earlier works such as the one by Sadeghi and Sui [4] assessed the effects of surface roughness in the form of a sinusoidal waviness, a line of work followed by many others [5,6] and more recently by Wang et al. [7]. Hooke [8] developed a perturbation analysis of the Reynolds equation as a fast analysis to access the global behavior of rough EHL contacts, under the assumption of small perturbation with respect to the smooth case.

* Corresponding author.
*E-mail address:* nicolas.fillot@insa-lyon.fr (N. Fillot).

https://doi.org/10.1016/j.triboint.2019.01.022
Received 28 August 2018; Received in revised form 9 January 2019; Accepted 19 January 2019
Available online 25 January 2019

Recent efforts have been focused on representing the surface *as it is*, that is, inputing the shape of realistic measured surfaces as data in the simulations, both for line and point contacts. Morales-Espejel at al [9] presented a fine-scale EHL model where the evolution of the surface is considered. TEHL contacts where both waviness and realistic surfaces are assessed were presented by Wang et al. [10]. Simulations with measured machined rough surfaces at different orientations were carried out by Zhu et al. [11], considering transient effects in TEHL contacts with a non-Newtonian lubricant. This line of work has also been followed by Refs. [12,13].

In all of these works the size of the contact region ranges from a few hundred micrometers to one milimeter, thus potentially holding hundreds of asperities. For other lubricated devices, such as the piston skirt/liner contact the number of asperities can rise to the thousands due to the dimensions of the domain, as shown by Zhu et al. [14]. Stochastic methods, averaging techniques and flow factors emerged to solve this issue and decouple the microscopic scale from the macroscopic scale, thus reducing the computational cost. From those, the most commonly adopted are Patir and Cheng's [15] flow factors, which are still commonly used in EHL [10,16,17].

All of these techniques are heuristic solutions to the formal approach which is homogenization. Averaged equations are developed with coefficients being computed in periodic cells (the so-called local problems) with the dimensions of the roughness wavelength. Furthermore, the flow factors can be formally defined, as done by Bayada [18]. The first homogenized results in EHL are due to Bayada et al. [19,20], where the authors dealt with a Newtonian fluid with piezoviscous effects and density variations. The linearity of the local problems, which is essential for the classic definition of the flow factors, relied on the asymptotic assumption.

Even though the surface roughness wavelength can be smaller in some orders of magnitude compared to the dimensions of the contact, the asymptotic assumption can lead to significant differences compared to the fine-scale solution. As shown by Venner and Lubrecht [21], high frequency roughness is almost undeformed by the fluid pressure, while the large wavelengths are largely affected. In an effort to incorporate the effects of a not-so-small wavelength, some authors have considered the deformations taking place in the local problems. This is the case of Budt et al. [22], who decoupled the microscopic from the macroscopic scale using a FE$^2$-type technique. Other authors preferred, in a more heuristic approach, to redefine the Patir and Cheng's flow factors considering the local deformations [23,24]. A precise definition of the homogenized EHL problem with finite-wavelength roughness and the corresponding flow factors is given by Scaraggi et al. [25,26]. However, they developed their approach for low contact pressures, and hence the lubricant properties are pressure-independent.

In the present work we propose a homogenized model for the stationary EHL line contact problem that takes into account piezoviscous effects and density variations with pressure, and where the size of the surface roughness is assumed to be non-infinitesimal. Micro-elastohydrodynamic effects were correctly captured in cases of technological interest. Although the developments were made for the one-dimensional stationary case in order to better assess the performance of the model, the extension to the two-dimensional transient case is not burdensome.

The article is outlined as follows: in Section 2 the fine-scale problem is presented in its non-dimensional form. Section 3 deals with generalities of the adopted homogenization technique, the asymptotic homogenized EHL model and the newly developed model. In order to assess the performance of the model herein proposed, a sensitivity analysis is carried out in Section 4. Finally, conclusions are drawn in Section 5.

## 2. Problem statement

We aim to solve stationary lubricated contacts in the elastohydrodynamic (EHL) regime considering piezoviscous effects and density variations with pressure. Cavitation effects are to be taken into account too. The geometry is the one seen in Fig. 1: two surfaces separated by a lubricating oil. As we are addressing a stationary problem, surface roughness can be present solely in the fixed surface.

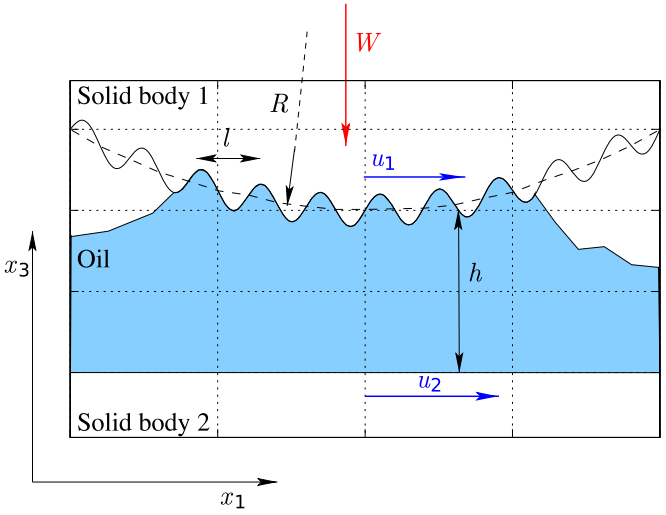


**Fig. 1.** Upper and lower finite solid bodies.

In this work we assume an infinitely long cylinder-on-plane contact. We assume that the computational domain $\Gamma^R$ where the fluid dynamics is going to be solved coincides with the $x_1$ line, Fig. 2. We begin by introducing the equation for the gap in the $x_3$ direction:

$$h(x_1) = h_0 + \frac{x_1^2}{2R} + h_r(x_1) + \delta(x_1) \tag{1}$$

where $R$ is the reduced radius of curvature in the $x_1$ direction of the line contact for the mean smooth surface, $h_0$ parametrizes the translation in the $x_3$ direction between both solids, $h_r$ describes the surface roughness (with a zero mean) and $\delta$ is a function representing the surface deformations due to the elastic behavior of the solids. $u_1$ and $u_2$ are respectively the velocities in the $x_1$ direction of the upper surface (1) and the lower surface (2) with respect to the contact center. We also assume elastic, isotropic, homogeneous solid bodies. The lower body moves in the $x_1$ direction with prescribed velocity while the upper one is free to move in the $x_3$ direction only (and thus $u_1 = 0$), its position being parametrized with $h_0$. The displacements $\boldsymbol{\delta}(x_1, x_3) = [\delta^{(1)}\ \delta^{(3)}]^T$ induced by the hydrodynamic pressure in the fluid $p(x_1)$ are given by the elastostatic equation

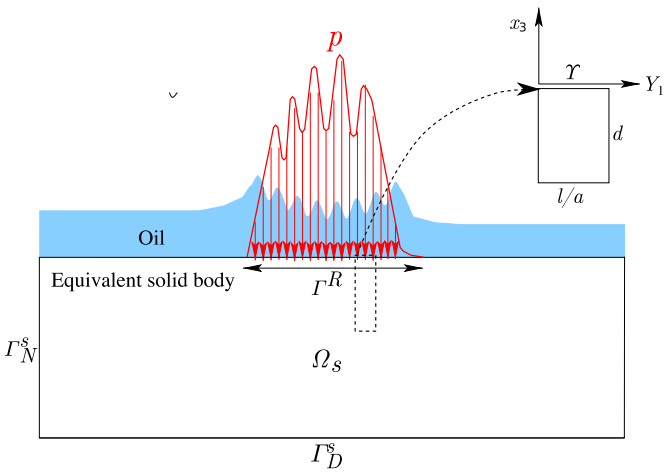


**Fig. 2.** A section of the computational domain.

$$\underline{\text{div}}\ \underline{\boldsymbol{\sigma}} = 0 \tag{2}$$

where $\underline{\boldsymbol{\sigma}}$ is the Cauchy stress tensor, which is given by Hooke's law

$$\underline{\boldsymbol{\sigma}} = \boldsymbol{D}\begin{bmatrix} \partial_{x_1}\delta^{(1)} \\ \partial_{x_3}\delta^{(3)} \\ \partial_{x_3}\delta^{(1)} + \partial_{x_1}\delta^{(3)} \end{bmatrix} \tag{3}$$

with

$$\boldsymbol{D} = \frac{E'}{(1+\nu')(1-2\nu')}\begin{bmatrix} 1-\nu' & \nu' & 0 \\ \nu' & 1-\nu' & 0 \\ 0 & 0 & \frac{1-2\nu'}{2} \end{bmatrix} \tag{4}$$

$E'$ and $\nu'$ being the Young's modulus and Poisson's coefficient of the equivalent material, which in terms of the properties of the bodies 1 and 2 are given by Ref. [27]:

$$E' = \frac{E_1^2E_2(1+\nu_2)^2 + E_1E_2^2(1+\nu_1)^2}{(E_1(1+\nu_2) + E_2(1+\nu_1))^2} \tag{5}$$

$$\nu' = \frac{E_1\nu_2(1+\nu_2) + E_2\nu_1(1+\nu_1)}{E_1(1+\nu_2) + E_2(1+\nu_1)} \tag{6}$$

From this it can be inferred that the deformations $\delta$ that affect the gap between the upper and lower solids in equation (1) are

$$\delta(x_1) = \underline{\boldsymbol{\delta}}(x_1, 0)\cdot \underline{\boldsymbol{e_3}} = \delta^{(3)}(x_1, 0) \tag{7}$$

where $\underline{\boldsymbol{e_3}}$ is the unitary vector in the $x_3$ direction. Equation (2) is solved in the equivalent domain $\Omega_s$, see Fig. 2. Notice that the same formulation can be applied even when the lower surface is rough, as we are considering the equivalent solid. The boundary conditions can be expressed as

- Dirichlet boundary condition: $\underline{\boldsymbol{\delta}} = \underline{\boldsymbol{\delta}}_D$ on $\Gamma_D^s$,
- von Neumann boundary condition: $\underline{\boldsymbol{\sigma}}\cdot\underline{\boldsymbol{n}} = 0$ on $\Gamma_N^s$,
- coupling term with Reynolds equation: $\underline{\boldsymbol{\sigma}}\cdot\underline{\boldsymbol{n}} = -p\underline{\boldsymbol{n}}$ on $\Gamma^R$.

where the boundary of the domain $\partial\Omega_s$ is split into complementary parts $\partial\Omega_s = \Gamma_D^s \cup \Gamma_N^s \cup \Gamma^R$. By taking the force exerted by the pressure along $x_3$ only we disregard the deformations caused by the shear stress in the $x_1$ direction and we assume small perturbations for the elastic problem. Here $\underline{\boldsymbol{n}}$ is the unitary normal to $\partial\Omega_s$.

It is assumed also that the thin film approximation is valid, and if we select the frame of reference on the upper surface, then the hydrodynamic pressure $p(x_1)$ is given by the following form of the Reynolds equation [28].

$$\frac{\partial}{\partial x_1}\left(u_m\rho h - \frac{\rho h^3}{12\mu}\frac{\partial p}{\partial x_1}\right) = 0 \tag{8}$$

Here the density $\rho = \rho(p)$ and the viscosity $\mu = \mu(p)$ are functions of the hydrodynamic pressure, and $u_m$ is the mean velocity $u_m = \frac{u_2+u_1}{2}$.

The load $W$ applied on the upper solid body must be balanced by the force exerted by the hydrodynamic pressure $p$:

$$W = \int_{\Gamma^R} p(x_1)dx_1 \tag{9}$$

Cavitation effects are introduced by means of a penalization method, as in Ref. [27]. The penalization method sets a source term $K_p p^-$ in the Reynolds equation (8), where $p^- = \min(p, 0)$, and $K_p > 0$ is a large penalization constant.

### 2.1. Non-dimensional form

We consider the following non-dimensionalizations and definitions:

$$X_1 = \frac{x_1}{a},\ X_3 = \frac{x_3}{a},\ \underline{\boldsymbol{\Delta}} = \frac{\underline{\boldsymbol{\delta}}}{a} \tag{10}$$

$$H = \frac{h}{a^2/R},\ H_0 = \frac{h_0}{a^2/R},\ H_r = \frac{h_r}{a^2/R},\ \Delta = \frac{\delta}{a^2/R} \tag{11}$$

$$\bar{u} = \frac{u_m}{u_r},\ \bar{\mu} = \frac{\mu}{\mu_r}\bar{\rho} = \frac{\rho}{\rho_r},\ P = \frac{p}{p_h},\ \underline{\boldsymbol{\Sigma}} = \frac{\underline{\boldsymbol{\sigma}}}{p_h} \tag{12}$$

Note that the non-dimensionalization for $\underline{\boldsymbol{\Delta}}$ and $\Delta$ are not the same. For a line contact [29] we select $a$ as the half width of the contact and $p_h$ as the maximum dry contact pressure of the Hertzian theory:

$$a = \sqrt{\frac{8WR}{\pi E_r}} \quad \text{and} \quad p_h = \frac{2W}{\pi a} \tag{13}$$

with $\frac{2}{E_r} = \frac{(1-\nu_1^2)}{E_1} + \frac{(1-\nu_2^2)}{E_2}$. Finally, $u_r$ is a reference velocity (when $u_m$ is constant, one can opportunely choose $u_r = u_m$), $\mu_r$ and $\rho_r$ are respectively the viscosity and density at atmospheric pressure.

This leads also to the following non-dimensional number:

$$\lambda = \frac{12u_r\mu_r R^2}{a^3 p_h} \tag{14}$$

Then the complete problem to be solved reads:

**Problem 1.** *Fine-scale reference problem* Given the constants (boundary conditions, geometry, material) $P_D$, $\underline{\boldsymbol{\Delta}}_D$, $\bar{u}$, $\lambda$, $K_p$, $E'/p_h$ and $\nu'$, the known functions $H_r(X_1)$, $\bar{\rho}(P)$ and $\bar{\mu}(P)$, find $H_0$, $P(X_1)$ and $\underline{\boldsymbol{\Delta}}(X_1, X_3)$ satisfying:

- Reynolds equation:

$$\frac{\partial}{\partial X_1}\left(\bar{u}\,\bar{\rho}H - \varepsilon\frac{\partial P}{\partial X_1}\right) + K_p P^- = 0 \tag{15}$$

where $\varepsilon = \frac{\bar{\rho}H^3}{\bar{\mu}\lambda}$, $P^- = \min(P, 0)$ and $H(X_1) = H_0 + \frac{X_1^2}{2} + H_r(X_1) + \Delta(X_1)$, and with the boundary conditions: $P(X_1) = P_D$ on $\Gamma^R$.

- Load balance:

$$\int_{\Gamma^R} P\,dX_1 = \frac{\pi}{2} \tag{16}$$

- Elastostatic problem:

$$\Delta(X_1) = \frac{R}{a}\underline{\boldsymbol{\Delta}}(X_1, 0)\cdot\underline{\boldsymbol{e_3}} \text{ on } \Gamma^R \tag{17}$$

where $\underline{\boldsymbol{\Delta}} = (\Delta^{(1)}, \Delta^{(3)})$ is the solution of

$$\underline{\text{div}}\ \underline{\boldsymbol{\Sigma}} = \boldsymbol{0} \tag{18}$$

with $\underline{\boldsymbol{\Sigma}}$ the Cauchy stress tensor

$$\underline{\boldsymbol{\Sigma}} = \frac{1}{p_h}\boldsymbol{D}\begin{bmatrix} \partial_{X_1}\Delta^{(1)} \\ \partial_{X_3}\Delta^{(3)} \\ \partial_{X_3}\Delta^{(1)} + \partial_{X_1}\Delta^{(3)} \end{bmatrix} \tag{19}$$

and boundary conditions $\underline{\boldsymbol{\Delta}} = \underline{\boldsymbol{\Delta}}_D$ on $\Gamma_D^s$, $\underline{\boldsymbol{\Sigma}}\cdot\underline{\boldsymbol{n}} = \boldsymbol{0}$ on $\Gamma_N^s$ and

$$\underline{\boldsymbol{\Sigma}}\cdot\underline{\boldsymbol{n}} = -P\underline{\boldsymbol{n}} \text{ on } \Gamma^R \tag{20}$$

### 2.2. Separation of scales

Assuming a periodic roughness of dimensional spatial period $l$, Fig. 3 illustrates that the surface is composed of a slow-varying part (dashed line) and a fast varying part (full line). With this in mind, the equation for the gap (1) can be rewritten as

$$H(X_1) = \tilde{H}(X_1) + \hat{H}(X_1) \tag{21}$$

where $\tilde{H}(X_1)$ represents the smooth, larger scale of the gap $H$

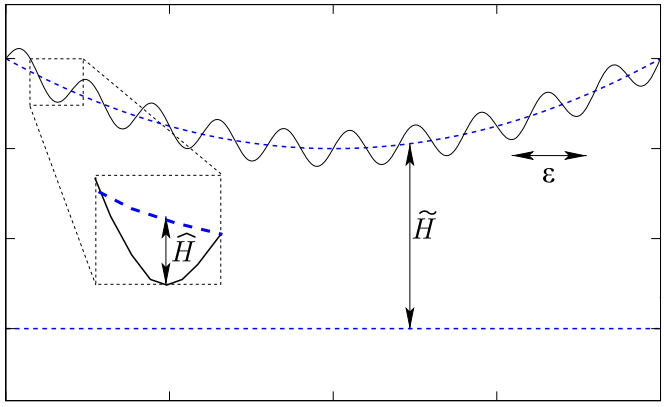


**Fig. 3.** Separating the macroscopic scale from the microscopic scale.

$$\tilde{H}(X_1) = H_0 + \frac{X_1^2}{2} + \tilde{\Delta}(X_1) \tag{22}$$

and $\hat{H}(X_1)$ the smaller scale, with periodicity $\varepsilon = l/a$ which is the non-dimensional wavelength of the roughness. $\varepsilon$ is also the scale ratio, expected to be small, between the roughness and the overall contact. Then $\hat{H}$ can be expressed as

$$\hat{H}(X_1) = H_r\left(\frac{X_1}{\varepsilon} - \xi\right) + \hat{\Delta}\left(X_1, \frac{X_1}{\varepsilon} - \xi\right) \tag{23}$$

Here $H_r$ represents the undeformed shape of the roughness, which we assume is periodic in $\varepsilon$, and $\xi$ is a phase shift. Both $\tilde{\Delta}$ and $\hat{\Delta}$ represent solid deformations in the large and small scale respectively, although their precise definition is postponed.

## 3. Homogenization of the elastohydrodynamic lubrication problem

The periodic roughness introduces a new variable

$$Y_1 = \frac{X_1}{\varepsilon} - \xi \tag{24}$$

which we can define in a non-dimensional domain $\Upsilon = [0,1]$ (see Fig. 2).

Then, the expression for the gap between the lubricated surfaces becomes

$$H(X_1, Y_1) = \tilde{H}(X_1) + \hat{H}(X_1, Y_1) \tag{25}$$

In the method of asymptotic expansions it is assumed that the hydrodynamic pressure can be expanded as:

$$P = P(X_1, Y_1) = P_0(X_1, Y_1) + \varepsilon P_1(X_1, Y_1) + \varepsilon^2 P_2(X_1, Y_1) + \ldots \tag{26}$$

where $P_0$, $P_1$, …are periodic in $Y_1$, and following (24) the derivative with respect to $X_1$ is replaced with

$$\frac{\partial}{\partial X_1} + \frac{1}{\varepsilon}\frac{\partial}{\partial Y_1} \tag{27}$$

As the term $P^-$ of the penalization method is not smooth, it cannot be expanded easily; the cavitation condition will be treated separately and is not considered at this point. Introducing (26) and (27) into equation (15) and considering the leading terms in the resulting expansion, that is, the terms in $\varepsilon^{-2}$, $\varepsilon^{-1}$ and $\varepsilon^0$ respectively we have

$$\frac{\partial}{\partial Y_1}\left(\varepsilon\frac{\partial P_0}{\partial Y_1}\right) = 0 \tag{28}$$

$$\frac{\partial}{\partial Y_1}(\bar{\rho}\,\bar{u}H) - \frac{\partial}{\partial X_1}\left(\varepsilon\frac{\partial P_0}{\partial Y_1}\right) - \frac{\partial}{\partial Y_1}\left(\varepsilon\frac{\partial P_0}{\partial X_1}\right) - \frac{\partial}{\partial Y_1}\left(\varepsilon\frac{\partial P_1}{\partial Y_1}\right) = 0 \tag{29}$$

$$\frac{\partial}{\partial X_1}(\bar{\rho}\,\bar{u}H) - \frac{\partial}{\partial X_1}\left(\varepsilon\frac{\partial P_0}{\partial X_1}\right) - \frac{\partial}{\partial X_1}\left(\varepsilon\frac{\partial P_1}{\partial Y_1}\right) - \frac{\partial}{\partial Y_1}\left(\varepsilon\frac{\partial P_1}{\partial X_1}\right) - \frac{\partial}{\partial Y_1}\left(\varepsilon\frac{\partial P_2}{\partial Y_1}\right) = 0 \tag{30}$$

and in the solid body, we have through the boundary conditions

$$\underline{\boldsymbol{\Sigma}}\cdot\boldsymbol{n} = -(P_0 + \varepsilon P_1 + \ldots)\boldsymbol{n} \text{ on } \Gamma^R \tag{31}$$

The linearity in this last equation and in the solid deformations problem allows us to expand the displacements $\underline{\boldsymbol{\Delta}}$ into

$$\underline{\boldsymbol{\Delta}} = \underline{\boldsymbol{\Delta}}(X_1, Y_1) = \underline{\boldsymbol{\Delta}}_0(X_1, Y_1) + \varepsilon\underline{\boldsymbol{\Delta}}_1(X_1, Y_1) + \varepsilon^2\underline{\boldsymbol{\Delta}}_2(X_1, Y_1) + \ldots \tag{32}$$

where each $\underline{\boldsymbol{\Delta}}_i$ is due to $P_i$, $i = 0,1,2, \ldots$ respectively, by expanding the linear elastic problem with respect to $\varepsilon$, and is $Y_1$-periodic. These developments allows the problem to be split as described in the following sections.

The load balance equation (16) is also expanded, leading to:

$$\int_{\Gamma^R} P_0\, dX_1 = \frac{\pi}{2} \tag{33}$$

$$\langle P_1\rangle = 0 \tag{34}$$

where $\langle\cdot\rangle$ denotes the average over the $\Upsilon$ domain.

### 3.1. The classical homogenized asymptotic (H-A) model

These classical results in asymptotic homogenization on the EHL problem are due to Bayada et al. [19] and are briefly recalled here. If we assume an infinitesimal $\varepsilon$, and also that the terms in $\varepsilon$, $\varepsilon^2$, …in equation (26) are negligible with respect to $P_0$, then expanding $H$, $\bar{\rho}$ and $\varepsilon$, it can be proven that equations (28)–(30) become

$$\frac{\partial}{\partial Y_1}\left(\varepsilon_0\frac{\partial P_0}{\partial Y_1}\right) = 0 \tag{35}$$

$$\frac{\partial}{\partial Y_1}(\overline{\rho_0}\,\bar{u}H) - \frac{\partial}{\partial X_1}\left(\varepsilon_0\frac{\partial P_0}{\partial Y_1}\right) - \frac{\partial}{\partial Y_1}\left(\varepsilon_0\frac{\partial P_0}{\partial X_1}\right) - \frac{\partial}{\partial Y_1}\left(\varepsilon_0\frac{\partial P_1}{\partial Y_1}\right) = 0 \tag{36}$$

$$\frac{\partial}{\partial X_1}(\overline{\rho_0}\,\bar{u}H) - \frac{\partial}{\partial X_1}\left(\varepsilon_0\frac{\partial P_0}{\partial X_1}\right) - \frac{\partial}{\partial X_1}\left(\varepsilon_0\frac{\partial P_1}{\partial Y_1}\right) - \frac{\partial}{\partial Y_1}\left(\varepsilon_0\frac{\partial P_1}{\partial X_1}\right) - \frac{\partial}{\partial Y_1}\left(\varepsilon_0\frac{\partial P_2}{\partial Y_1}\right) = 0 \tag{37}$$

with

$$\bar{\rho}_0 = \bar{\rho}(P_0),\ \bar{\mu}_0 = \bar{\mu}(P_0),\ \varepsilon_0 = \frac{\bar{\rho}_0 H^3}{\bar{\mu}_0\lambda} \tag{38}$$

$$H = \tilde{H} + H_r,\ \tilde{H} = H_0 + \frac{X_1^2}{2} + \Delta_0 \tag{39}$$

#### 3.1.1. Microscopic problem

From equation (35) it can be inferred that $P_0 = P_0(X_1)$, and thus $\tilde{\Delta} = \Delta_0(X_1)$ are macroscopic displacements computed on $\Omega_s$. Notice that there are only macroscopic deformations in the expression for the clearance $H$ (39), i.e. $\hat{\Delta} = 0$. Taking this into account, equation (36) becomes linear on $P_1$:

$$\frac{\partial}{\partial Y_1}(\overline{\rho_0}\,\bar{u}H) - \frac{\partial}{\partial Y_1}\left(\varepsilon_0\frac{\partial P_0}{\partial X_1}\right) - \frac{\partial}{\partial Y_1}\left(\varepsilon_0\frac{\partial P_1}{\partial Y_1}\right) = 0 \tag{40}$$

This problem for the microscopic pressure $P_1$ is determined up to a constant of $X_1$. This constant is fixed using the micro load balance equation (34).

#### 3.1.2. Macroscopic problem

Averaging (37) leads to:

$$\frac{\partial}{\partial X_1}(\overline{\rho_0}\,\bar{u}\langle H\rangle) - \frac{\partial}{\partial X_1}\left(\langle\varepsilon_0\rangle\frac{\partial P_0}{\partial X_1}\right) - \frac{\partial}{\partial X_1}\left\langle\varepsilon_0\frac{\partial P_1}{\partial Y_1}\right\rangle = 0 \tag{41}$$

This is the equation for the macroscopic pressure $P_0$. Since $H_0$ is also an unknown in the expression of the film thickness $H$, an additional equation to close the problem is the macro load balance (33).

As mentioned previously, the elastostatic problem is only derived at macroscale: $\Delta_0(X_1) = \frac{R}{a}\underline{\boldsymbol{\Delta}}_0(X_1, 0)\cdot \underline{\boldsymbol{e_3}}$ on $\Gamma^R$, where $\underline{\boldsymbol{\Delta}}_0 = (\Delta_0^{(1)}, \Delta_0^{(3)})$ is the solution of

$$\underline{\text{div}}\ \underline{\boldsymbol{\Sigma}}_0 = \mathbf{0} \tag{42}$$

with

$$\underline{\boldsymbol{\Sigma}}_0 = \frac{1}{p_h}\boldsymbol{D}\begin{bmatrix} \partial_{X_1}\Delta_0^{(1)} \\ \partial_{X_3}\Delta_0^{(3)} \\ \partial_{X_3}\Delta_0^{(1)} + \partial_{X_1}\Delta_0^{(3)} \end{bmatrix} \tag{43}$$

and boundary conditions $\underline{\boldsymbol{\Delta}}_0 = \underline{\boldsymbol{\Delta}}_D$ on $\Gamma_D^s$, $\underline{\boldsymbol{\Sigma}}_0\cdot\underline{\boldsymbol{n}} = \mathbf{0}$ on $\Gamma_N^s$ and

$$\underline{\boldsymbol{\Sigma}}_0\cdot\underline{\boldsymbol{n}} = -P_0\underline{\boldsymbol{n}} \text{ on } \Gamma^R \tag{44}$$

### 3.1.3. Relocalization

Although the homogenized asymptotic model is developed for a infinitesimal $\varepsilon$, it is still expected that it can approximate the solution of the reference problem with a finite wavelength $\varepsilon_0$ in certain situations, such as when $\varepsilon_0$ and roughness amplitude are small enough. Thus, the hydrodynamic pressure can be reconstructed as

$$P(X_1) \simeq P_0(X_1) + \varepsilon_0 P_1(X_1, Y_1) = P_0(X_1) + \varepsilon_0 P_1\left(X_1, X_1 - \varepsilon_0\lfloor\frac{X_1}{\varepsilon_0}\rfloor - \xi\right) \tag{45}$$

where $\lfloor\cdot\rfloor$ is the floor function, returning the greatest integer less or equal than $(\cdot)$.

## 3.2. The homogenized μ-EHL model

The classical asymptotic homogenization does not involve piezo-viscous effects nor elasticity at the microscopic scale. It is only valid if $\varepsilon_0 P_1$ is very small when compared to $P_0$. This constitutes a limitation of this approach, leading to inaccurate solutions for severe loading conditions, i.e., when the film thickness is not very large when compared to the roughness amplitude. The homogenized $\mu$-EHL model is intended to overcome these limitations. We assume the same expansion of equation (26), however, we will not develop the constitutive laws $\bar{\rho}$, $\bar{\mu}$ and the coefficient $\varepsilon$ in equations (28)–(30). For those terms, we will consider the finite roughness wavelength $\varepsilon_0$ such that

$$\bar{\rho} = \bar{\rho}(P_0 + \varepsilon_0 P_1),\ \bar{\mu} = \bar{\mu}(P_0 + \varepsilon_0 P_1),\ \varepsilon = \frac{\bar{\rho}H^3}{\bar{\mu}\lambda} \tag{46}$$

and

$$H = \tilde{H} + \hat{H},\ \tilde{H} = H_0 + \frac{X_1^2}{2} + \Delta_0,\ \hat{H} = H_r + \varepsilon_0\Delta_1 \tag{47}$$

with $\Delta_1$ being microscopic displacements to be fully defined in the following sections. Here the higher order terms in $\varepsilon_0^2$, $\varepsilon_0^3$, …, are still neglected.

### 3.2.1. Microscopic problem

As in the classical asymptotic model, from equation (35) it can be deduced again that $P_0 = P_0(X_1)$ and thus $\underline{\boldsymbol{\Delta_0}} = \underline{\boldsymbol{\Delta_0}}(X_1)$ too. The microscopic problems for the pressure are now the non-linear equation in $P_1$

$$\frac{\partial}{\partial Y_1}(\bar{\rho}\,\bar{u}H) - \frac{\partial}{\partial Y_1}\left(\varepsilon\frac{\partial P_0}{\partial X_1}\right) - \frac{\partial}{\partial Y_1}\left(\varepsilon\frac{\partial P_1}{\partial Y_1}\right) = 0 \tag{48}$$

Again, the problem is determined up to a constant of $X_1$, however, contrary to the homogenized asymptotic model this constant affects also the solution of the macro pressure $P_0$, as can be seen from the dependency of $\bar{\mu}$ and $\bar{\rho}$ with $P_1$.

The assumption of a non-negligible $\varepsilon_0 P_1$ term leads to non-negligible displacements $\varepsilon_0\Delta_1$. An elastic problem (yet to be defined) must be solved, with a boundary condition with pressure $P_1$ on $\Upsilon \times \{0\}$. Notice that $P_1 = P_1(X_1, Y_1)$ introduces the fast variable $Y_1$ in the elastic deformations problem.

Due to the zero average of $P_1$ over $\Upsilon$, Saint Venant's principle implies that the deformations induced by this force will be localized, i.e., they won't propagate far away from the area of application of $P_1$. This assumption allows us to solve these micro-deformations in a reduced domain $\Upsilon \times [0, d]$ (see Fig. 2), where the length $d$ is determined by the roughness wavelength $\varepsilon_0$ and the equivalent Poisson's coefficient $\nu'$ (assuming $\nu'$ not close to 0.5 for witch Saint Venant's principle is not valid).

This new problem in $\Upsilon \times [0, d]$ (see Fig. 2) is in the variables $Y_1$ and $Y_3 = X_3/\varepsilon_0$. Notice that at each point $X_1$ an independent problem has to be solved in $\Upsilon \times [0, d]$, which is parametrized by $P_0$, $\tilde{H}$ and $\partial_{X_1}P_0$ in contrast with the microscopic problems of the classical model, which only depend on two parameters, $\tilde{H}$ and $\partial_{X_1}P_0$. Then the equation for the elastic deformations $\underline{\boldsymbol{\Delta_1}}(X_1, Y_1, Y_3) = (\Delta_1^{(1)}, \Delta_1^{(3)})$ is

$$\underline{\text{div}}_Y\ \underline{\boldsymbol{\Sigma}}_1 = 0 \tag{49}$$

where $\underline{\text{div}}_Y$ is the divergence operator with respect to the coordinates $(Y_1, Y_3)$, and $\underline{\boldsymbol{\Sigma}}_1$ is the micro Cauchy stress tensor in the solid $\Upsilon \times [0, d]$:

$$\underline{\boldsymbol{\Sigma}}_1 = \frac{1}{p_h}\boldsymbol{D}\begin{bmatrix} \partial_{Y_1}\Delta_1^{(1)} \\ \partial_{Y_3}\Delta_1^{(3)} \\ \partial_{Y_3}\Delta_1^{(1)} + \partial_{Y_1}\Delta_1^{(3)} \end{bmatrix} \tag{50}$$

In $\{0\} \times [0, d]$ and $\{\varepsilon_0\} \times [0, d]$ the only requirement that we have is periodicity of $\underline{\boldsymbol{\Delta}}_1$ in the $Y_1$ variable:

$$\underline{\boldsymbol{\Delta_1}}(X_1, 0, Y_3) = \underline{\boldsymbol{\Delta_1}}(X_1, \varepsilon_0, Y_3) \tag{51}$$

We assume that $\Upsilon \times \{d\}$ is sufficiently far away from the localized deformations at $\Upsilon \times \{0\}$, so that we can set the Dirichlet boundary conditions:

$$\underline{\boldsymbol{\Delta_1}} = \boldsymbol{C} \text{ on } Y \times \{d\} \tag{52}$$

where $\boldsymbol{C}$ is a constant to be determined with $\langle\Delta_1\rangle = 0$, and the boundary condition coupling the micro-elastostatics to the micro Reynolds equation:

$$\underline{\boldsymbol{\Sigma}}_1\cdot\underline{\boldsymbol{n}} = -P_1\underline{\boldsymbol{n}} \text{ on } \Gamma^R \tag{53}$$

Particularly, we are interested at the deformations at the surface $\Upsilon \times \{0\}$

$$\Delta_1(X_1, Y_1) = \varepsilon_0\frac{R}{a}\underline{\boldsymbol{\Delta_1}}(X_1, Y_1, 0)\cdot\underline{\boldsymbol{e_3}} \tag{54}$$

where the factor $\varepsilon_0$ stands from the difference between the scaling factors of the elastic problem and the gap $H$ in the microscopic Reynolds equation in $\underline{\boldsymbol{e_3}}$ direction.

### 3.2.2. Macroscopic problem

Taking the average of equation (37) we now obtain:

$$\frac{\partial}{\partial X_1}(\bar{u}\langle\bar{\rho}H\rangle) - \frac{\partial}{\partial X_1}\left(\langle\varepsilon\rangle\frac{\partial P_0}{\partial X_1}\right) - \frac{\partial}{\partial X_1}\left(\langle\varepsilon\frac{\partial P_1}{\partial Y_1}\rangle\right) = 0 \tag{55}$$

We assume the pressure boundary conditions $P_D$ to be only a function of the slow variable $X_1$, so it reads

$$P_0(X_1) = P_D \text{ on } \partial\Gamma^R \tag{56}$$

The macroscale displacements $\Delta_0$ come from the solution of the elastostatic equation with $P_0$ as von Neumann boundary conditions, as in the classical asymptotic model.

### 3.2.3. Dealing with cavitation in the two-scale model

For the homogenized models we propose to introduce penalization

terms in both the microscale and the macroscale equations, taking into account that the condition for cavitation $P_0 + \varepsilon_0 P_1 \geq 0$ can be traduced into a restriction for the microscopic pressure

$$P_1 \geq -\frac{P_0}{\varepsilon_0} \tag{57}$$

However, imposing the cavitation condition only in the microscopic pressure is not feasible. A physical argument against it is that the large negative pressures arising in the divergent part of the lubricated contact could not be suppressed by the small pressures developed in small or even moderately small roughness. Hence, constraints will be set both on the macroscopic and microscopic pressures. Then, the penalization term for the macroscopic equation is $K_p P_0^-$ with

$$P_0^- = \min(P_0, 0) \tag{58}$$

and the one for the microscopic equation is $K_p P_1^-$, with $P_1^-$ defined with

$$P_1^- = \min\left(P_1 + \frac{P_0}{\varepsilon_0}, 0\right) \tag{59}$$

while it is not necessary that the constant $K_p$ be the same for both penalization terms. It should be noticed that the penalization method allows small negative pressures to take place. If $P_0 \leq 0$ at a certain point in the domain, the condition set by equation (57) will lead to an incompatibility with $\langle P_1 \rangle = 0$. In order to avoid this we will set $P_1 \equiv 0$ at all the points $X_1$ of the macroscopic domain where $P_0 \leq 0$. This is consistent with the straight application of cavitation unilateral constraint: indeed when a macro cavitation takes place (i.e. $P_0 = 0$) the constraint $\langle P_1 \rangle = 0$ together with $P_1 \geq -\frac{P_0}{\varepsilon_0} = 0$ leads also to $P_1 = 0$.

Thus, we can summarize the $\mu$-EHL model as:

**Problem 2.** *Homogenized* μ*-EHL problem* Given the constants (boundary conditions, geometry, material) $P_D$, $\boldsymbol{\Delta}_D$, $\bar{u}$, $\varepsilon_0$, λ, $K_p$, $E'/P_h$ and $\nu'$, the known functions $H_r(Y_1)$, $\bar{\rho}(P_0 + \varepsilon_0 P_1)$ and $\bar{\mu}(P_0 + \varepsilon_0 P_1)$, find the macroscopic quantities $H_0$, $P_0(X_1)$, $\Delta_0(X_1)$ and the microscopic corrections $P_1(X_1, Y_1)$, $\Delta_1(X_1, Y_1)$ (with $\langle P_1 \rangle = \langle \Delta_1 \rangle = 0$ and $Y_1$-periodicity) satisfying:

- the two-scale Reynolds equations with $\varepsilon = \frac{\bar{\rho} H^3}{\bar{\mu}\lambda}$:

$$\frac{\partial}{\partial X_1}(\bar{u}\langle\bar{\rho}H\rangle) - \frac{\partial}{\partial X_1}\left(\langle\varepsilon\rangle\frac{\partial P_0}{\partial X_1}\right) - \frac{\partial}{\partial X_1}\left(\langle\varepsilon\frac{\partial P_1}{\partial Y_1}\rangle\right) + K_p P_0^- = 0 \tag{60}$$

$$\frac{\partial}{\partial Y_1}(\bar{\rho}\bar{u}H) - \frac{\partial}{\partial Y_1}\left(\varepsilon\frac{\partial P_0}{\partial X_1}\right) - \frac{\partial}{\partial Y_1}\left(\varepsilon\frac{\partial P_1}{\partial Y_1}\right) + K_p P_1^- = 0 \tag{61}$$

- this last one being superseded by $P_1(X_1, Y_1) \equiv 0$ if $P_0(X_1) \leq 0$, and the film thickness $H$ being (47).
- the load balance equation (33)
- the two-scale elastostatic problem (42, 43, 44) and (49, 50, 53)

## 4. Validation of the homogenized $\mu$-EHL model

Let us first outline the fine-scale reference problem. The non-dimensional computational domain for the Reynolds equation is defined in $\Gamma^R = [-4,2]$; the elastic body is defined on $\Omega_s = [-35,25] \times [-60,0]$, see Fig. 4.

The boundary conditions are set as $P_D = 0$, $\boldsymbol{\Delta}_D = 0$; the velocity is set to $\bar{u} = 1$.

The non-dimensional expression for the laws governing the compressibility of the fluid and the piezoviscosity chosen for the numerical tests are

$$\bar{\rho} = 1 + \frac{c_A\, p}{1 + c_B\, p} \tag{62}$$

$$\bar{\mu} = \left(\frac{\mu_\infty}{\mu_r}\right)^{1-\left(1+\frac{p}{\gamma}\right)^c} \tag{63}$$

the first one being a proposal of Dowson and Higginson [30] and the former by Roelands [31], where $\mu_\infty = 6.31 \times 10^{-5}$ Pa.s and $\gamma = 1.961 \times 10^8$ Pa are constants of the model. Here we have chosen $c_A = 6 \times 10^{-10}$ Pa$^{-1}$, $c_B = 2 \times 10^{-9}$ Pa$^{-1}$, $\mu_r = 0.004$ Pa.s, and $c = 0.5$.

The non-dimensional penalty method constant here taken is $K_p = 1000$ for every simulation.

On the upper surface we set sinusoidal periodic textures, given by the equation:

$$H_r(X_1) = A\sin\left(2\pi\left(\frac{X_1}{\varepsilon_0} - \xi\right)\right) = A\sin(2\pi Y_1) = H_r(Y_1) \tag{64}$$

where $A$ is the non-dimensional roughness amplitude.

In order to define a maximum value for the amplitude $A$ of the roughness in the simulations, we will use the film thickness ratio

$$\Lambda = \frac{H_{\min}}{\sigma} \tag{65}$$

where $\sigma$ is the root mean square value of the non-dimensional combined roughness of both surfaces in contact, and thus here equal to $\sigma = \frac{\sqrt{2}}{2}A$. The minimum film thickness is $H_{\min} = \min_{\Gamma^R} H$.

For elastohydrodynamic lubrication some authors [28,32] suggest $3 < \Lambda < 10$. Here we will take a minimum film thickness ratio of $\Lambda = 5.66$, which gives us $A = 0.25 H_{\min}$. As $H_{\min}$ is not known a priori, then the maximum $A$ will be taken as a fraction of $H_{\min,A=0}$, that is, the minimum film thickness of the smooth problem (no surface roughness):

$$A_{\text{rel}} = \frac{A}{H_{\min,A=0}} \tag{66}$$

To assess the differences between the reference, the homogenized asymptotic and the homogenized $\mu$-EHL models, several values of the roughness wavelength $\varepsilon_0$ and amplitude $A$ will be explored.

What remains to define the problem are three non-dimensional quantities: λ, $E'/p_h$ and $\nu'$. The λ parameter is a measure of the relevance of the fluid dynamics effects compared to the solid deformations, while $E'/p_h$ gives us a measure of the importance of the solid deformations. A larger $E'/p_h$ means a stiffer solid or a lower load imposed on the lubricated contact. In every numerical test we will adopt a fixed value of $\nu' = 0.3$, while the other two parameters will take values corresponding to cases of technological interest. This choice is based on the fact that the Poisson ratio of typical metallic materials is around 0.3 and that the solution will not vary significantly for those values. In order to put the results into the perspective of the tribology community, along with the λ, $E'/p_h$ and $\nu'$ parameters that define each problem we will provide the Moes-Venner parameters [33].

$$M = \frac{W}{\sqrt{2u_m E_r R \mu_r}}, \quad L = \alpha E_r^{3/4}\left(\frac{2u_m\mu_r}{R}\right)^{1/4} \tag{67}$$

with $\alpha = c\ln(\mu_r/\mu_\infty)/\gamma$ being the pressure-viscosity coefficient. Fig. 5 shows the Moes parameters for which simulations were ran, with

$$H_m^M = \frac{H_{\min}}{a^2/R}\sqrt{\frac{E_r}{2u_m\mu_r R}} \tag{68}$$

At each point a substantial number of roughness configurations were appraised.

To illustrate this in a more tangible manner, these values are consistent with the parameters of Table 1.

The Reynolds and the elastostatic equations were discretized by means of the finite element method, with second order Lagrange elements. The microscopic problems of the homogenized models were solved at each node of the mesh of the macroscopic problem in a FE$^2$-homogenization manner (such as in Ref. [34]). This leads to a large

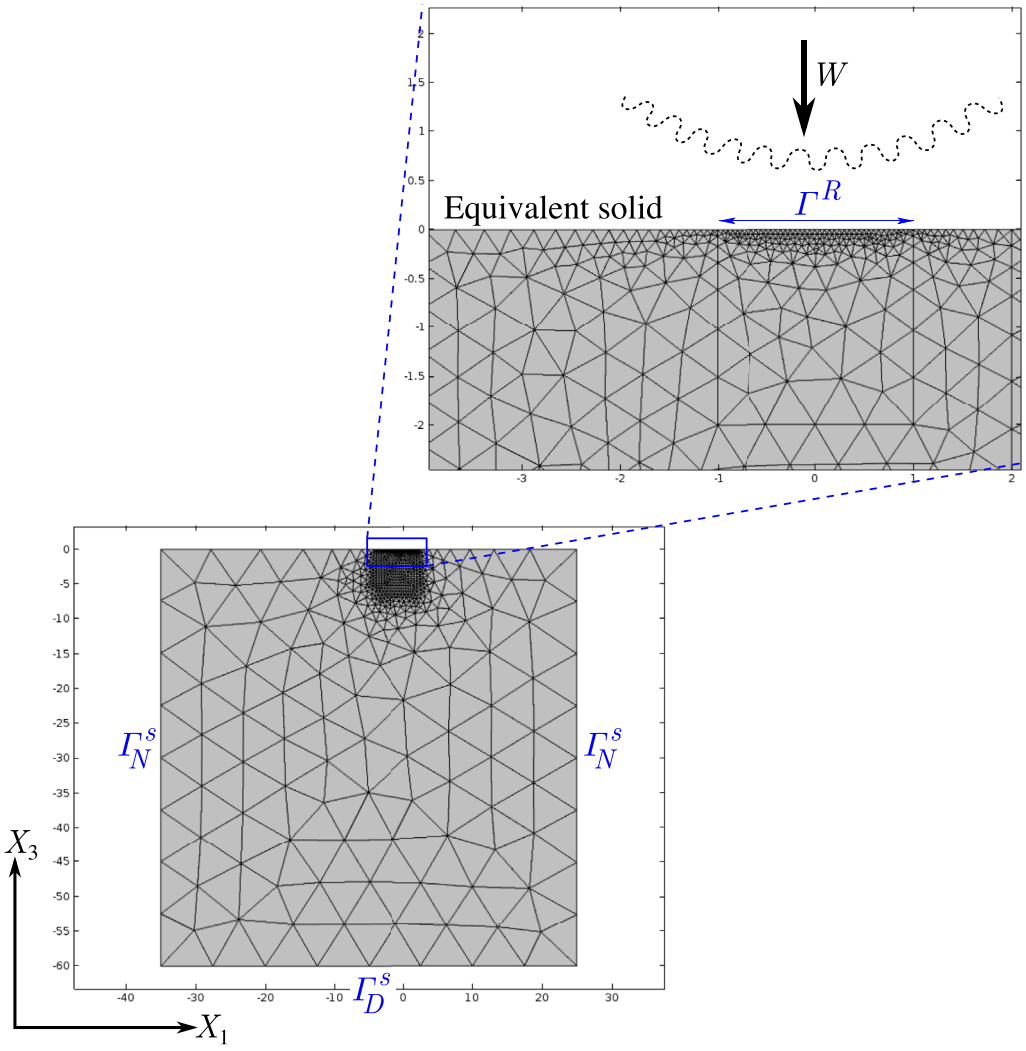


**Fig. 4.** A finite element mesh on the equivalent solid (domain $\Omega_s$) and on the domain where the Reynolds equation is solved ($\Gamma^R$).

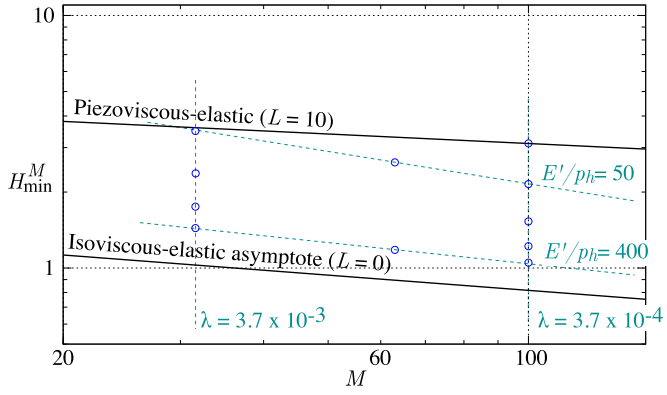


**Fig. 5.** Numerical tests were carried out for the $M$, $L$ ($\lambda$, $E'/p_h$) values marked by the blue circles. The dashed lines represent configurations of constant $E'/p_h$ and $\lambda$. At each point several roughness configurations ($A_{\text{rel}}$, $\varepsilon_0$, $\xi$) were assessed. (For interpretation of the references to color in this figure legend, the reader is referred to the Web version of this article.)

number of degrees of freedom, however, as we aim to assess the accuracy of the model here proposed we want to eliminate sources of error, e.g. the ones coming from the decoupling of the macro-scale equations from the microscopic equations. Nonetheless, this will restrict our capacity to solve problems for small $\varepsilon_0$ values.

**Table 1**
Parameters corresponding to the cases depicted in Fig. 5.

| M | L | λ | $E'/p_h$ | $p_h$ /GPa | a/m | R/m | $u_r$ /(m/s) |
|---|---|---|---|---|---|---|---|
| 100 | 0.66 | $3.7 \times 10^{-4}$ | 400 | 0.25 | 0.025 | 5.51 | 1 |
| 100 | 1.33 | $3.7 \times 10^{-4}$ | 200 | 0.50 | 0.031 | 0.34 | 1 |
| 100 | 2.65 | $3.7 \times 10^{-4}$ | 100 | 1.00 | $3.9 \times 10^{-3}$ | 0.022 | 1 |
| 100 | 5.30 | $3.7 \times 10^{-4}$ | 50 | 2.00 | $4.9 \times 10^{-5}$ | $1.3 \times 10^{-3}$ | 1 |
| 31.6 | 1.18 | $3.7 \times 10^{-3}$ | 400 | 0.25 | 0.025 | 5.51 | 10 |
| 31.6 | 2.36 | $3.7 \times 10^{-3}$ | 200 | 0.50 | $3.1 \times 10^{-3}$ | 0.34 | 10 |
| 31.6 | 4.72 | $3.7 \times 10^{-3}$ | 100 | 1.00 | $3.9 \times 10^{-4}$ | 0.022 | 10 |
| 31.6 | 9.43 | $3.7 \times 10^{-3}$ | 50 | 2.00 | $4.9 \times 10^{-5}$ | $1.3 \times 10^{-3}$ | 10 |
| 63.3 | 0.83 | $9.3 \times 10^{-4}$ | 400 | 0.25 | 0.025 | 5.51 | 2.5 |
| 63.3 | 6.67 | $9.3 \times 10^{-4}$ | 50 | 2.00 | $4.9 \times 10^{-5}$ | $1.3 \times 10^{-3}$ | 2.5 |

A monolithic Newton-Raphson solver is used for the non-linear systems and all linear system of equations are solved using direct methods. Results were computed using commercial software (COMSOL Multiphysics$^R$ version 5.2a).

Due to the lack of existence of known analytical solutions, all simulated cases will be compared against the reference solution computed in a very fine mesh where the $[-1,1]$ region of $\Gamma^R$ is discretized into finite elements of size $\Delta X_1 = 1 \times 10^{-4}$. This discretization leads to 743 134 degrees of freedom in the reference problem and negligible differences in the solution with respect to even finer meshes. For the

homogenized models, the $[-1,1]$ region of $\Gamma^R$ of the macro-scale equations was discretized with finite elements of the size of the roughness wavelength: $\Delta X_1 = \varepsilon_0$, and enough finite elements in the micro-problems to ensure mesh convergence. The error computed for a certain field $Q$ is

$$e_Q = \frac{\|Q - Q_{\text{ref}}\|_{L^2(\Omega)}}{\|Q_{\text{ref}}\|_{L^2(\Omega)}} \tag{69}$$

where $Q_{\text{ref}}$ is the mesh-converged fine-scale solution and the norms are $L^2$-norms taken in the corresponding domain $\Omega$.

### 4.1. Scope of the homogenized asymptotic (H-A) and homogenized μ-EHL models

If the roughness wavelength $\varepsilon_0$ and amplitude $A_{\text{rel}}$ are small enough, then the classical homogenized asymptotic and the $\mu$-EHL give similar models; in particular they are expected to be accurate approximations of the reference problem. We are interested in the more realistic case of a small but not infinitesimal roughness wavelength $\varepsilon_0$ nor amplitude $A_{\text{rel}}$. To assess the model ranges of validity, we start at a low $L$ value of 0.66 and $M = 100$. Errors in pressure $e_P$ are presented for several $\varepsilon_0$ and $A_{\text{rel}}$ pairs on Table 2.

As can be seen in Table 2, the errors for the classical homogenized asymptotic model (H-A) grow rapidly with both variables. Fig. 6-(b) for $\varepsilon_0 = 0.05$ and 6-(d) show how the model disregards the microscopic deformations at the asperity level, which leads to microscopic pressures larger than the ones of the reference solution. In behalf of this, the micro-pressures grow with $\varepsilon_0$, as shown in Fig. 6-(a) and 6-(c), which correspond to errors of 12.1% and 55.1% respectively. This explains the trends displayed in Table 2. Larger values of $L$ induce even larger errors, which leads to the conclusion that the classical homogenized asymptotic model will return satisfactory results only for very low $L$ values. This shows its inadequacy to approximate the reference solution when $\varepsilon_0$ is not infinitesimal. On the other hand, the errors attained with the $\mu$-EHL model are low, and in every computed case in Table 2 they are below 0.5%. They tend to grow slightly with the roughness amplitude, however, due to the low errors with differences in the tenths of percent a clear trend is not perceived while varying $\varepsilon_0$.

### 4.2. A sensitivity study

The accuracy of the homogenized $\mu$-EHL approximation is here analyzed. As discussed in the previous section, the errors grow with the amplitude $A$ as expected, however, for the other parameters that define the problem the dependency is not trivial. First, a discussion on the influence of the roughness phase $\xi$ is carried on. This is done by selecting a pair $\lambda$, $E'/p_h$, or equivalently a pair $M$,$L$ and assessing the errors in pressure and clearance, for different $\varepsilon_0$ values and a fixed $A_{\text{rel}} = 0.25$. Thereafter, a sensitivity study on the errors in pressure for varying $\lambda$ and $E'/p_h$ is performed.

**Table 2**
Percentage errors in pressure $e_P$, relative to the reference solution for $E'/p_h = 400$ and $\lambda = 3.7 \times 10^{-4}$ for several roughness wavelengths $\varepsilon_0$ and amplitudes $A_{\text{rel}}$. These cases correspond to Moes parameters of $M = 100$ and $L = 0.66$.

| (a) H-A | | | |
|---|---|---|---|
| $\varepsilon_0 \backslash A_{\text{rel}}$ | 0.05 | 0.15 | 0.25 |
| 0.05 | 2.67 | 7.75 | 12.1 |
| 0.1 | 6.13 | 17.7 | 27.3 |
| 0.2 | 13.4 | 35.7 | 55.1 |
| (b) $\mu$-EHL | | | |
| $\varepsilon_0 \backslash A_{\text{rel}}$ | 0.05 | 0.15 | 0.25 |
| 0.05 | 0.12 | 0.21 | 0.37 |
| 0.1 | 0.11 | 0.23 | 0.29 |
| 0.2 | 0.11 | 0.22 | 0.30 |

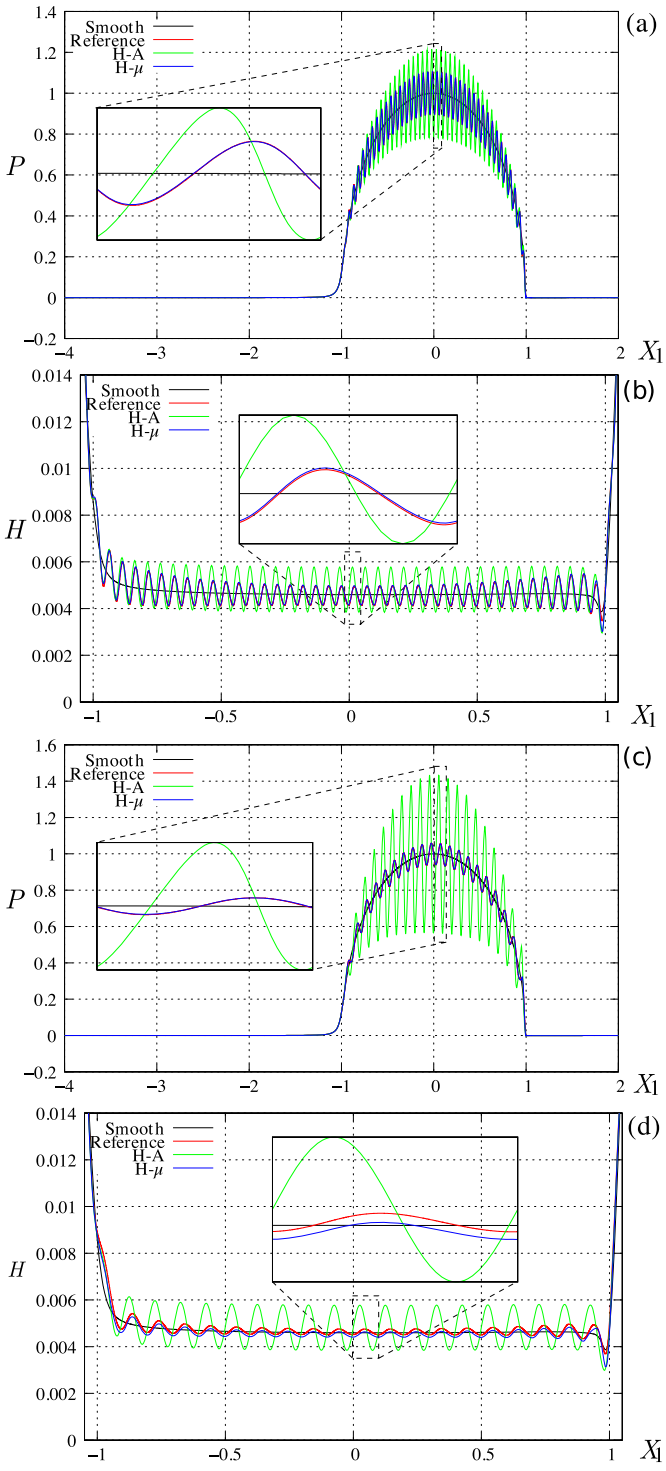


**Fig. 6.** Pressure (a,c) and clearance (b,d) for the homogenized asymptotic (H–A) and the homogenized $\mu$-EHL model (H-$\mu$) for parameters $M = 100$, $L = 0.66$, $A_{\text{rel}} = 0.25$, $\varepsilon_0 = 0.05$ (top) and $\varepsilon_0 = 0.2$ (bottom).

#### 4.2.1. Sensitivity in pressure and clearance to the phase ξ

The feeding conditions at the entrance of the lubricated contact are determined by the relative position of the roughness to it. This has a particular impact on the cleareance, as shown in an extensive study in

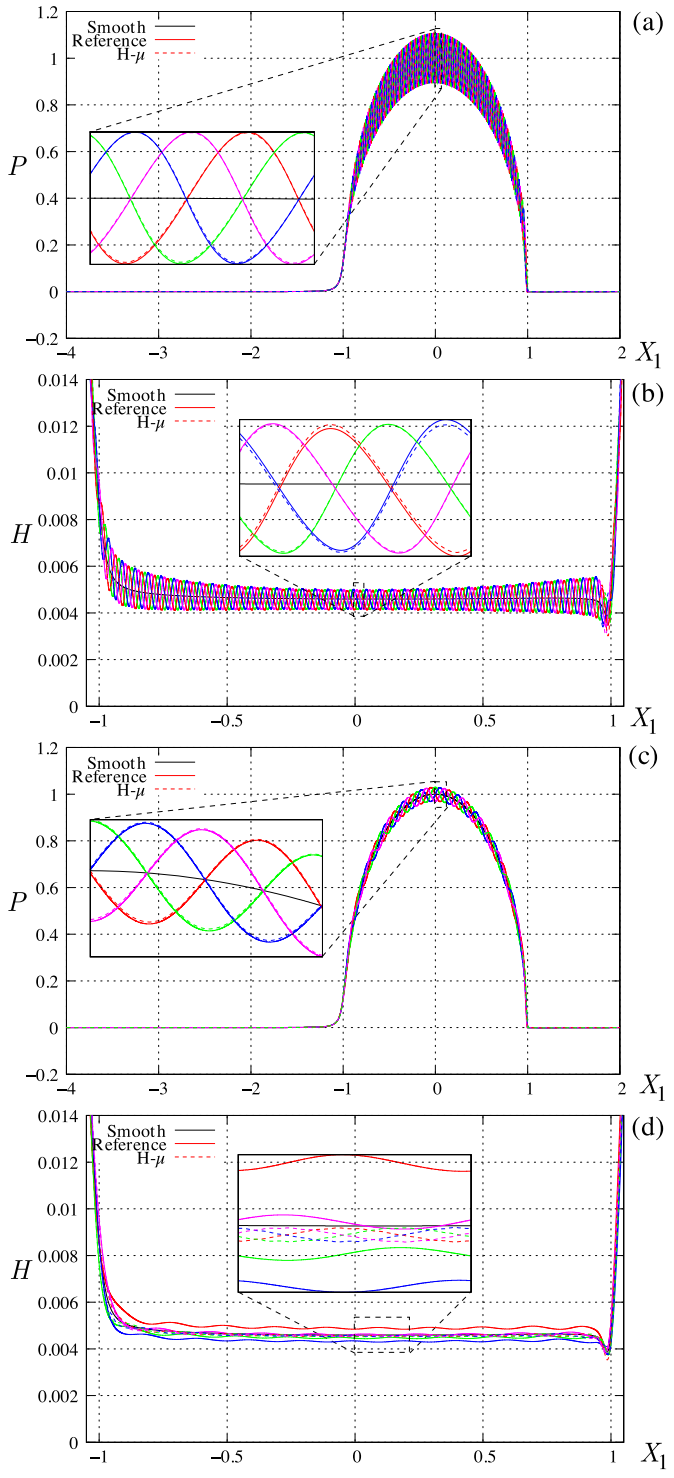


**Fig. 7.** Pressure (a,c) and clearance (b,d) for the homogenized $\mu$-EHL model (dashed lines) and the reference solution (full lines) for parameters $M = 100$, $L = 0.66$, $A_{\text{rel}} = 0.25$, $\varepsilon_0 = 0.05$ (top) and $\varepsilon_0 = 0.1$ (bottom). Solutions were computed for phase $\xi$ values of 0, 0.25, 0.5 and 0.75.

EHL line contacts in Ref. [35]. This effect is controlled by the deformation of the roughness, which is itself governed by the *generalized wavelength* (Venner et al. [36])

$$V = \varepsilon_0 \frac{M^{3/4}}{L^{1/2}} \tag{70}$$

High $V$ values lead to higher roughness deformations. This can be achieved either by a large wavelength $\varepsilon_0$ or by a large $\frac{M^{3/4}}{L^{1/2}}$ ratio. From the parameters in Table 1, $M = 31.6$, $L = 9.43$ attain the lowest $V$ while $M = 100$, $L = 0.66$ the highest. Errors in pressure and clearance will be compared for this set of parameters.

Let us first look at the point $M = 100$, $L = 0.66$ from the Moes graph, for $A_{\text{rel}} = 0.25$ and $\varepsilon_0 = 0.05$. Fig. 7(a) and (b) show both the pressure and the clearance for the reference (full lines), smooth and the homogenized $\mu$-EHL (dashed lines) solutions for several phase values of $\xi = 0$, 0.25, 0.5 and 0.75. Curves computed for the same phase $\xi$ appear in the same color. In order to compute a representative error for the clearance $H$, we restricted $e_H$ to the interval $[-1,1]$ in all cases. The approximation both in clearance and pressure for all phases $\xi$ is excellent, the maximum errors being $e_P = 0.37\%$ and $e_H = 1.13\%$.

If the roughness wavelength is increased to $\varepsilon_0 = 0.1$ we have the results of Fig. 7(c) and (d). The maximum and minimum errors in pressure are $e_P = 0.35\%$ and $e_P = 0.29\%$ respectively. This can be seen in Fig. 7(c): for each reference solution there is a closely matching homogenized pressure curve computed for the same $\xi$ value. However, this is not the case for the clearance curves. The ones corresponding to the reference solution in Fig. 7(d) present some dispersion while the $\mu$-EHL ones are clustered around an average, the maximum error being $e_H = 4.2\%$ and the minimum $e_H = 1.8\%$.

This behavior can be explained in the following manner: the averages taken with respect to the fast variable $Y_1$ in order to develop the homogenized macroscopic equations induce an independency on the macroscopic quantities on the roughness phase $\xi$. Hence, the average values of pressure ($P_0$) and clearance ($\tilde{H}$) are insensitive to the phase. No significant differences are seen in pressure due to the restriction imposed by the load balance equation, which sets the average value of the pressure in each periodic cell. However, there is no equivalent restriction for the clearance.

Let us turn now to the results for $M = 31.6$, $L = 9.43$ which are shown in Fig. 8. For the sake of clarity, only the solution for $\xi = 0$ is shown in pressure. Fig. 8-(a) and 8-(b) depict the results for $\varepsilon_0 = 0.05$. An excellent approximation can be seen in both pressure and clearance. The maximum error in pressure for the phases computed is $e_P = 2.3\%$, while it is $e_H = 1.5\%$ in clearance. The differences between the homogenized $\mu$-EHL curves and the reference ones are small and limited to the inlet and outlet regions in the case of the pressure curves. Notice how in every case the micro-elastohydrodynamic behavior is captured by the homogenized model. If we turn now to Fig. 8-(c) and 8-(d) we can see again an excellent fit on the pressure (maximum $e_P = 2.5\%$) while some small differences are seen in the clearance curves, with a maximum error $e_H = 2.2\%$. These results, that of a higher error in clearance with larger deformations (larger $V$) correlate well with the results of Couhier [35] and Venner [36]. It is to be noticed that the errors $e_P$ and $e_H$ are more sensitive to $\varepsilon_0$ than to $M$ and $L$.

#### 4.2.2. *Pressure sensitivity to λ and $E'/p_h$*

What remains to be appraised is the sensitivity on the pressure to the two main non-dimensional parameters controlling the problem: λ and $E'/p_h$. In order to do that, the phase and amplitude are fixed to $\xi = 0$ and $A_{\text{rel}} = 0.25$.

We set fixed values of $\lambda = 3.7 \times 10^{-4}$ ($M = 100$) and $\lambda = 3.7 \times 10^{-3}$ ($M = 31.6$) and vary $E'/p_h$. Table 3-(a) shows that for a lower λ value, errors slightly increase when decreasing $E'/p_h$. The sensitivity increases with larger λ values, as can be seen in a comparison between Tables 3-(a) and (a'). The largest errors in pressure, which remain lower than 3%, take place for larger λ and lower $E'/p_h$ values. It is worthy of note the low sensitivity to the roughness wavelength, at least for the range of $\varepsilon_0$ values analyzed here.

If $E'/p_h$ is fixed at values of 400 and 50 and λ varies, we have the results of Table 4. Table 4-(a) shows that errors stay below 0.5% for $E'/p_h = 400$, and that they are quite insensitive to $\varepsilon_0$. A higher sensitivity is seen for $E'/p_h = 50$ (Table 4-(a')), as errors marginally increase

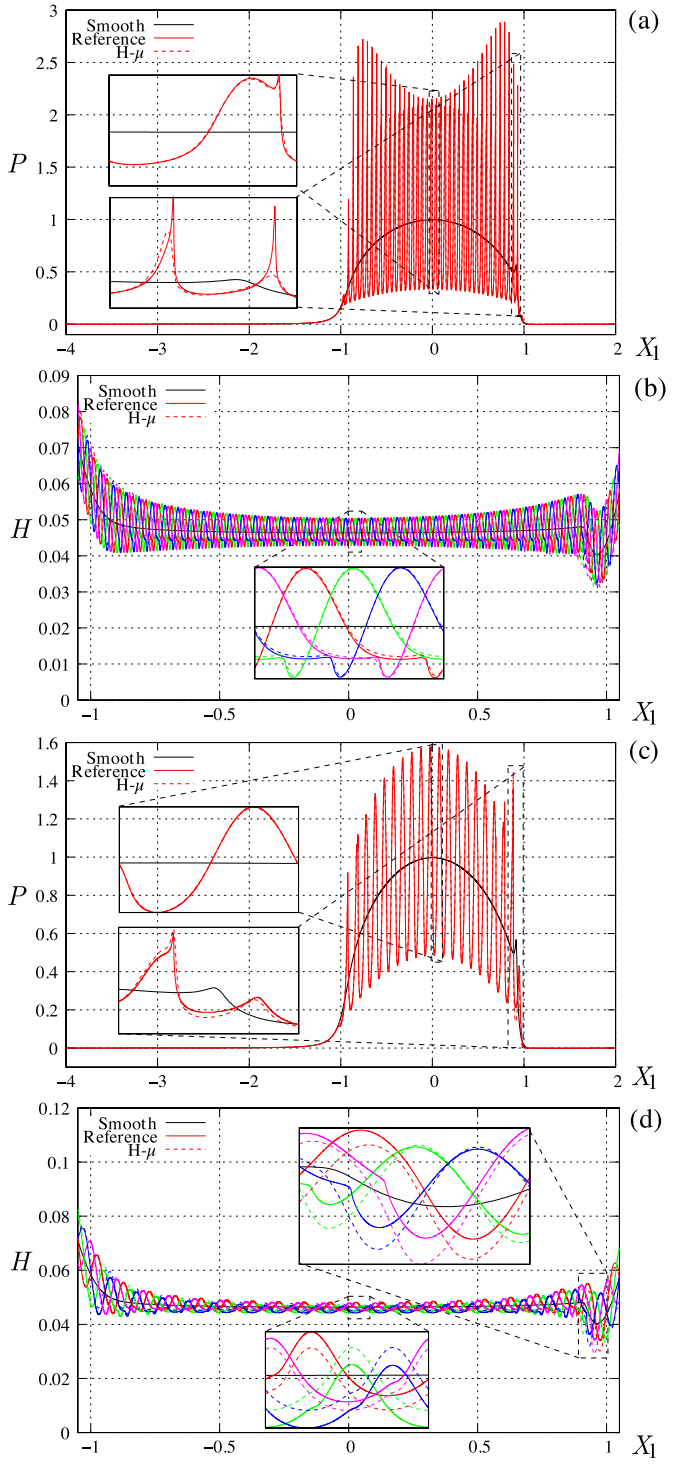


**Fig. 8.** Pressure (a,c) and clearance (b,d) for the homogenized $\mu$-EHL model (do) and the reference solution for parameters $M = 31.6$, $L = 9.43$, $A_{\text{rel}} = 0.25$, $\varepsilon_0 = 0.05$ (top) and $\varepsilon_0 = 0.1$ (bottom). Solutions were computed for phase $\xi$ values of 0, 0.25, 0.5 and 0.75. For simplicity, the pressure curves are shown only for $\xi = 0$.

with $\varepsilon_0$. In summary, it can be stated that errors are low for higher $E'/p_h$ ratios and lower λ values and almost insensitive to $\varepsilon_0$, while somewhat larger for lower $E'/p_h$ and higher λ.

## 5. Conclusions

A new homogenized approximation of the rough elastohydrodynamic lubrication problem was presented. This new approximation takes into account the effects of a non-negligible microscopic pressure, compared to the classical periodic asymptotic homogenization where these are neglected. As a result of this assumption local deformations must be computed in the microscopic periodic cells as well as the effects of the local pressure in density and viscosity. These are the main differences with the asymptotic approach. This allows to

**Table 3**
(a, a') Percentage errors in pressure $e_p$ relative to the reference solution for varying $E'/p_h$ values and fixed λ values. The amplitude $A_{\text{rel}} = 0.25$ in all cases. (b,b') Moes parameters for the cases of Tables (a,a').

(a) Percentage errors for $\lambda = 3.7 \times 10^{-4}$

| $\varepsilon_0 \backslash E'/p_h$ | 400 | 200 | 100 | 50 | 26.5 |
|---|---|---|---|---|---|
| 0.05 | 0.36 | 0.41 | 0.52 | 0.90 | 1.41 |
| 0.1 | 0.29 | 0.37 | 0.43 | 1.12 | 1.52 |
| 0.2 | 0.30 | 0.25 | 0.39 | 0.88 | 1.40 |

(b) Moes parameters

| $E'/p_h$ | 400 | 200 | 100 | 50 | 26.5 |
|---|---|---|---|---|---|
| $M$ | 100 | 100 | 100 | 100 | 100 |
| $L$ | 0.66 | 1.33 | 2.65 | 5.3 | 10 |

(a') Percentage errors for $\lambda = 3.7 \times 10^{-3}$

| $\varepsilon_0 \backslash E'/p_h$ | 400 | 200 | 100 | 50 |
|---|---|---|---|---|
| 0.05 | 0.28 | 0.38 | 1.07 | 2.15 |
| 0.1 | 0.80 | 1.00 | 1.16 | 2.44 |
| 0.2 | 1.06 | 1.64 | 2.01 | 2.63 |

(b') Moes parameters

| $E'/p_h$ | 400 | 200 | 100 | 50 |
|---|---|---|---|---|
| $M$ | 31.6 | 31.6 | 31.6 | 31.6 |
| $L$ | 1.18 | 2.36 | 4.72 | 9.43 |

**Table 4**
(a,a') Percentage errors in pressure $e_p$ relative to the reference solution for varying λ values and fixed $E'/p_h$ values. The amplitude $A_{\text{rel}} = 0.25$ in all cases. (b,b') Moes parameters for the cases of Tables (a,a').

(a) Percentage errors for $E'/p_h = 400$

| $\varepsilon_0 \backslash \lambda$ | $3.7 \times 10^{-4}$ | $9.25 \times 10^{-4}$ | $3.7 \times 10^{-3}$ |
|---|---|---|---|
| 0.05 | 0.36 | 0.28 | 0.39 |
| 0.1 | 0.29 | 0.80 | 0.60 |
| 0.2 | 0.30 | 1.06 | 0.52 |

(b) Moes parameters

| $\lambda$ | $3.7 \times 10^{-4}$ | $9.25 \times 10^{-4}$ | $3.7 \times 10^{-3}$ |
|---|---|---|---|
| $M$ | 100 | 63.25 | 31.6 |
| $L$ | 0.66 | 0.83 | 1.18 |

(a') Percentage errors for $E'/p_h = 50$

| $\varepsilon_0 \backslash \lambda$ | $3.7 \times 10^{-4}$ | $9.25 \times 10^{-4}$ | $3.7 \times 10^{-3}$ |
|---|---|---|---|
| 0.05 | 0.90 | 1.38 | 2.15 |
| 0.1 | 1.12 | 1.10 | 2.44 |
| 0.2 | 0.88 | 1.22 | 2.63 |

(b') Moes parameters

| $\lambda$ | $3.7 \times 10^{-4}$ | $9.25 \times 10^{-4}$ | $3.7 \times 10^{-3}$ |
|---|---|---|---|
| $M$ | 100 | 63.26 | 31.63 |
| $L$ | 5.30 | 6.67 | 9.43 |

extend the applicability of homogenization methods to more realistic conditions.

The differences of the solutions obtained with the new homogenized model and the solution of the reference problem were assessed in parametric studies. Errors in pressure are below or equal to 2% and remarkably insensitive to the roughness amplitude and wavelength for a wide range of Moes parameters, namely for $L < 6$. Errors in pressure grow and are slightly more sensitive to the amplitude of the roughness and the roughness wavelength when $L > 6$, but remain below 3% for the range $31.6 \leq M \leq 100$, $0.66 \leq L \leq 10$.

Errors in clearance grow with larger $M$ and lower $L$ values but remain below 5%, that is with larger micro-deformations. They are more sensitive to the roughness wavelength than to $M$, $L$. Micro-elastohydrodynamic effects are correctly captured by the newly developed homogenized method.

The model here presented was restricted to the one-dimensional case and stationary conditions in order to better assess its efficiency. The extension to the two-dimensional case and transient conditions will be the object of future research.

## Acknowledgments

The authors are grateful to Total Marketing & Services for its financial support. D.Dureisseix, J. Raisin and N. Fillot wish to dedicate this article to the memory of Huco Checo, the first author, who left us too soon.

## References

[1] Pei S, Xu H, Shi F. A deterministic multiscale computation method for rough surface lubrication. Tribol Int 2016;94:502–8. https://doi.org/10.1016/j.triboint.2015.10.005.
[2] Gropper D, Wang L, Harvey TJ. Hydrodynamic lubrication of textured surfaces: a review of modeling techniques and key findings. Tribol Int 2016;94:509–29. https://doi.org/10.1016/j.triboint.2015.10.009.
[3] Raisin J, Fillot N, Dureisseix D, Vergne P, Lacour V. Characteristic times in transient thermal elastohydrodynamic line contacts. Tribol Int 2015;82:472–83. https://doi.org/10.1016/j.triboint.2014.02.022.
[4] Sadeghi F, Sui PC. Thermal elastohydrodynamic lubrication of rolling/sliding contacts. J Tribol 1990;112(2):189–95. https://doi.org/10.1115/1.2920241.
[5] Chang L. Traction in thermal elastohydrodynamic lubrication of rough surfaces. J Tribol 1992;114(1):186–91. https://doi.org/10.1115/1.2920859.
[6] Wang J, Kaneta M. A study on starved micro-thermal elastohydrodynamic lubrication in simple sliding circular contacts. Proc IME J J Eng Tribol 2007;221(3):209–21. https://doi.org/10.1243/13506501JET223.
[7] Wang J, Lubrecht AA, Sperka P, Omasta M, Kaneta M. Effect of high slide-roll ratio on thermal elastohydrodynamic lubrication in line contacts with surface waviness. Proc IME J J Eng Tribol 2015;229(5):568–77. https://doi.org/10.1177/1350650114556397.
[8] Hooke CJ. The behaviour of low-amplitude surface roughness under line contacts. Proc IME J J Eng Tribol 1999;213(4):275–85. https://doi.org/10.1243/1350650991542668.
[9] Morales-Espejel GE, Brizmer V, Piras E. Roughness evolution in mixed lubrication condition due to mild wear. Proc IME J J Eng Tribol 2015;229(11):1330–46. https://doi.org/10.1177/1350650115577404.
[10] Wang X, Liu Y, Zhu D. Numerical solution of mixed thermal elastohydrodynamic lubrication in point contacts with three-dimensional surface roughness. J Tribol 2017;139(1):011501https://doi.org/10.1115/1.4032963.
[11] Zhu D, Wang J, Wang QJ. On the Stribeck curves for lubricated counterformal contacts of rough surfaces. J Tribol 2015;137(2):021501https://doi.org/10.1115/1.4028881.
[12] Akchurin A, Bosman R, Lugt P, van Drogen M. On a model for the prediction of the friction coefficient in mixed lubrication based on a load-sharing concept with measured surface roughness. Tribol Lett 2015;59(1):19. https://doi.org/10.1007/s11249-015-0536-z.
[13] Pu W, Wang J, Zhu D. Friction and flash temperature prediction of mixed lubrication in elliptical contacts with arbitrary velocity vector. Tribol Int 2016;99:38–46. https://doi.org/10.1016/j.triboint.2016.03.017.
[14] Zhu D, Cheng HS, Arai T, Hamai K. A numerical analysis for piston skirts in mixed lubrication Part I: basic modeling. J Tribol 1992;114(3):553–62. https://doi.org/10.1115/1.2920917.
[15] Patir N, Cheng HS. An average flow model for determining effects of three-dimensional roughness on partial hydrodynamic lubrication. Journal of Lubrication Technology 1978;100(1):12–7. https://doi.org/10.1115/1.3453103.
[16] Masjedi M, Khonsari M. On the effect of surface roughness in point-contact EHL: formulas for film thickness and asperity load. Tribol Int 2015;82:228–44. https://doi.org/10.1016/j.triboint.2014.09.010.
[17] Larsson R. Modelling the effect of surface roughness on lubrication in all regimes. Tribol Int 2009;42(4):512–6. https://doi.org/10.1016/j.triboint.2008.07.007.
[18] Bayada G. Application of the homogenization method to Reynolds roughness. Developments in numerical and experimental methods applied to tribology: proceedings of the 10th Leeds–Lyon symposium on tribology. Elsevier; 2014. p. 53.
[19] Bayada G, Martin S, Vázquez C. Homogenization of a nonlocal elastohydrodynamic lubrication problem: a new free boundary model. Math Model Methods Appl Sci 2005;15(12):1923–56. https://doi.org/10.1142/S0218202505001023.
[20] Bayada G, Martin S, Vázquez C. Micro-roughness effects in (elasto)hydrodynamic lubrication including a mass-flow preserving cavitation model. Tribol Int 2006;39:1707–18. https://doi.org/10.1016/j.triboint.2006.03.003.
[21] Venner CH, Lubrecht AA. An engineering tool for the quantitative prediction of general roughness deformation in EHL contacts based on harmonic waviness attenuation. Proc IME J J Eng Tribol 2005;219(5):303–12. https://doi.org/10.1243/135065005X33973.
[22] Budt M, Temizer I, Wriggers P. A computational homogenization framework for soft elastohydrodynamic lubrication. Comput Mech 2012;49(6):749–67. https://doi.org/10.1007/s00466-012-0709-7.
[23] Kim TW, Cho YJ. The flow factors considering the elastic deformation for the rough surface with a non-Gaussian height distribution. Tribol Trans 2008;51(2):213–20. https://doi.org/10.1080/10402000701730502.
[24] Sahlin F, Larsson R, Almqvist A, Lugt PM, Marklund P. A mixed lubrication model incorporating measured surface topography. Part 1: theory of flow factors. Proc IME J J Eng Tribol 2009;224(4):335–51. https://doi.org/10.1243/13506501jet658.
[25] Scaraggi M, Carbone G, Persson BNJ, Dini D. Lubrication in soft rough contacts: a novel homogenized approach. Part I-Theory. Soft Matter 2011;7(21):10395–406. https://doi.org/10.1039/C1SM05129F.
[26] Scaraggi M, Dorogin L, Angerhausen J, Murrenhoff H, Persson BNJ. Elastohydrodynamics for soft solids with surface roughness: transient effects. Tribol Lett 2017;65(3):95. https://doi.org/10.1007/s11249-017-0878-9.
[27] Habchi W, Eyheramendy D, Vergne P, Morales-Espejel G. Stabilized fully-coupled finite elements for elastohydrodynamic lubrication problems. Adv Eng Software 2012;46(1):4–18. https://doi.org/10.1016/j.advengsoft.2010.09.010.
[28] Hamrock B, Schmid S, Jacobson B. Fundamentals of fluid film lubrication. New York: Marcel Dekker; 2004. https://doi.org/10.1201/9780203021187.
[29] Johnson KL. Contact mechanics. Cambridge University Press; 1987.
[30] Dowson D, Higginson GR. Elasto-hydrodynamic lubrication, International series on materials science and technology. Pergamon Press; 1977. https://doi.org/10.1016/C2013-0-05764-7.
[31] Roelands CJA. Correlational aspects of the viscosity-temperature-pressure relationships of lubricating oils. Druk. V.R.B.; 1966.
[32] Davim J. Tribology in manufacturing technology. Springer; 2012.
[33] Venner CH. Multilevel solution of the EHL line and point contact problems. 1991.
[34] Feyel F, Chaboche JL. Multi-scale non-linear FE2 analysis of composite structures: damage and fiber size effects. Rev Eur Des Eléments Finis 2001;10(2–4):449–72. https://doi.org/10.1080/12506559.2001.11869262.
[35] Couhier F. Influence des rugosités de surface sur les mécanismes de lubrification du contact élastohydrodynamique cylindre-plan, Ph.d. thesis. INSA Lyon; 1996.
[36] Venner CH, Couhier F, Lubrecht AA, Greenwood JA. Amplitude reduction of waviness in transient EHL line contacts. Tribology series, vol. 32. Elsevier; 1997. p. 103–12. https://doi.org/10.1016/S0167-8922(08)70440-1.